Numerical and experimental study on prediction of thermal history and residual deformation of double-sided fillet welding

P Biswas[1]*, **M M Mahapatra[2],** and **N R Mandal[1]**
[1]Department of Ocean Engineering and Naval Architecture, Indian Institute of Technology, West Bengal, India
[2]Department of Mechanical Engineering, KIIT University, Bhubaneswar, India

Abstract: Distortions occur in almost every arc welded joint. The nature of the created distortion depends on several parameters including the welding speed, plate thickness, welding current, voltage, and restraints applied to the job. The distortions and thermal history of a joint can be measured experimentally but the measurement procedure may be costly and time-consuming. In the present work a numerical elasto-plastic thermomechanical model has been developed for predicting the thermal history and resulting angular distortions of submerged arc welded double-sided fillet joints. A moving distributed heat source was used in the finite element modelling of the double-sided fillet welding to create a realistic simulation of the process. The effect of filler metal deposition was taken into account by implementing a birth-and-death process for the elements. The transient temperature distributions were predicted using temperature-dependent material properties. The angular distortion profiles were predicted based on the transient temperature distributions of the fillet welds. The model yielded results that match the experimental values (with a variation of 5–10 per cent for the maximum values of the distortions and a variation of 8 per cent for peak temperatures).

Keywords: 3D finite element analysis, moving distributed heat source, transient thermal analysis, angular distortion, non-linear elasto-plastic analysis, submerged arc welding

1 INTRODUCTION

Submerged arc welding (SAW) is widely used in industries such as shipbuilding where thick plates need to be welded. Sequentially welded double-sided fillets are widely used in fabrication processes. However, studies using thermomechanical analysis to predict the thermal history and distortions of SAW double-sided fillet welds are rarely found in literature. There is, therefore a need for a simple thermomechanical model to predict the thermal history and distortion patterns for SAW of double-sided fillet welds.

Residual transverse, lateral, angular, and bowing deformations are present in every fusion welded joint and generally for fillet joints the angular distortion is the predominant deformation. The accurate prediction of welding distortions is extremely difficult because of the thermal and mechanical conditions created during the welding process including locally high temperatures, temperature-dependent material properties, and a moving heat source. However, the finite element simulation of welding is highly effective in predicting thermomechanical behaviour.

In this work the SAW processing of a double-sided fillet has been studied using numerical and experimental approaches for predicting temperature distributions and resulting angular distortions. A simplified finite element model has been developed for the three-dimensional (3D) analysis of fillet joints to allow the prediction of angular distortions for a moving distributed heat source. For this, first the temperature distribution patterns were obtained and compared with experimental results. Then a thermomechanical analysis was carried out to isolate angular distortion patterns.

---

*Corresponding author: Department of Ocean Engineering, and Naval Architecture, Indian Institute of Technology, Kharagpur, West Bengal 721 302, India.
email: panu012@yahoo.co.in

Rosenthal [1, 2] provided one of the earliest approaches to the development of an analytical solution of the heat flow problem during welding. His approach is based on using the conduction heat transfer to predict the shape of the weld pool for two-dimensional (2D) and 3D welds. This approach provides reasonable predictions for points far away from the heat source, however, the predictions are not accurate enough for regions close to the heat source.

Finite element methods have been successfully used to predict temperature distributions, residual stresses, and distortions. Brown and Song [3] proposed 3D thermomechanical solutions to predict distortion patterns. Kamala and Goldak [4] investigated the error created by using a 2D approximation in the heat transfer analysis of welds. Michaleris and DeBiccari [5] used finite element modelling to successfully predict the distortions created in a welding process of steel using temperature-dependent material properties and kinematic work hardening of the steel. Tsai and Cheng [6] investigated the distortion mechanism and the effects of welding sequence on thin panel distortions using a finite element analysis approach. Teng *et al.* [7] investigated the residual stresses and distortion of T-joint fillet welds using a 2D finite element analyses approach. Jung and Tsai [8] modelled the angular distortion of T-joints using a plasticity-based distortion analysis. McDill *et al.* [9] compared the weld residual stresses obtained for 2D plane strain and 3D analyses. Murakawa *et al.* [10] predicted the hot cracking of a weld using temperature-dependent interface elements. Mahapatra *et al.* [11] modelled the effect of the position of tack weld constraints on the angular distortions created in one-sided fillet welds created by SAW. It is clear from this literature review that the thermal history and the resulting distortions in a welded joint are strongly affected by various parameters and their interactions.

A large number of models exist to predict temperature distributions, residual stresses, and distortions in the welded joints, though most of them have concentrated on 2D approximations of the 3D problem. The need for a 3D simulation process that is able to fully simulate the behaviour of a complete welded structure has been highlighted in [3], [4], and [11].

2 THERMOMECHANICAL ANALYSIS

2.1 Thermal modelling

In the present work a 3D finite element model is developed to analyse the heat transfer and temperature distribution in double-sided fillet welding using SAW. Models for both conduction and convection processes are available in the literature. It is clear from the literature survey that the heat transfer mechanism in the molten pool is extremely complex. Although some progress has recently been made towards a realistic modelling of convective heat transfer, these efforts are still directed towards simpler and generalized cases. In arc welding, except for a small volume of metal, most of the portion of the workpiece remains in the solid state. Therefore, a 3D conduction model was considered for the heat flow analysis and the resulting temperature distribution over the entire plate [11, 12]. A schematic of the double-sided fillet weld with the axis system used in the finite element model is shown in Fig. 1. The areas bounded by weld lines 1-2-4-3-1 and 5-6-8-7-5 (Fig. 1) were considered to be S_1 in the finite element model and is where the moving heat source was applied. Except for these areas (i.e. areas
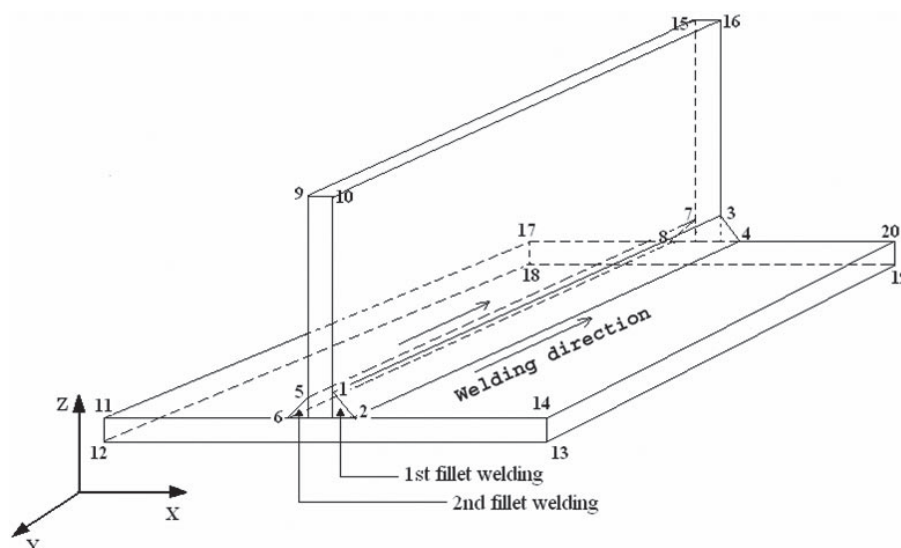

Fig. 1 Schematic diagram of the fillet joint weld with numbered corner points

bounded by weld lines 1-2-4-3-1 and 5-6-8-7-5; Fig. 1) other areas of the fillet joints were considered to be S_2 where convection loss was assumed as in the literature [**11**].

The governing differential equation for heat conduction for a homogeneous, isotropic solid without heat generation in the rectangular coordinate system (x, y, z) can be expressed as

$$\frac{\partial}{\partial x}\left(k\frac{\partial T}{\partial x}\right) + \frac{\partial}{\partial y}\left(k\frac{\partial T}{\partial y}\right) + \frac{\partial}{\partial z}\left(k\frac{\partial T}{\partial z}\right) = \rho c\frac{\partial T}{\partial t} \qquad (1)$$

2.1.1 Boundary conditions

The finite element modelling of the thermal behaviour during SAW performed in the present investigation is governed by equation (1) and is subjected to the following three boundary conditions.

1. A specified initial temperature for the welding that covers all the finite elements of the model

$$T = T_\infty \quad \text{for } t = 0 \qquad (2)$$

    where T_∞ is the ambient temperature.
2. The heat flux due to the welding arc is applied over the surface of the weld zone (surface S_1)

$$\begin{aligned} q_n &= -q_{sup} \\ -k\frac{\partial T}{\partial n} &= -q_{sup} \quad \text{for } t > 1 \end{aligned} \qquad (3)$$

3. Convection loss only occurs at surface S_2

$$-k\frac{\partial T}{\partial n} = -h_f(T_\infty - T) \quad \text{for } t > 0 \qquad (4)$$

To avoid a sharp change in the value of the specific heat, the enthalpy was used as a material property. This was done by defining the enthalpy of the material as a function of temperature [**11**, **12**]. To simulate filler material deposition for each welding pass a birth-and-death technique was used for each element. For this, initially all the elements in the weld regions were deactivated and sequentially activated as the heat source moved along the weld areas of the first and second fillet welding as per the direction of welding shown in Fig. 1.

2.1.2 Assumptions made in the thermal model

As far as possible the actual welding conditions were considered in the thermal model. However, the following assumptions were still required.

1. All the thermal properties were considered to be a function of the temperature.

2. Linear Newtonian convection cooling was considered on all the surfaces.
3. The heat loss due to radiation, conduction through the electrode, and heat consumed by burning of the flux and melting of the electrode were accounted for by the arc energy transfer efficiency parameter η [**13**]. In the present study a value of 0.9 was taken for η for the SAW process.
4. A constant convection coefficient of 15 W/m²K was considered [**7**].
5. Heat flux was considered as a load.
6. A birth-and-death technique was used in this model to simulate the formation of a weld bead through metal deposition. The proposed method does not remove elements to achieve the 'death' effect. Instead, the method deactivates an element by multiplying its stiffness by a large reduction factor. The mass and energy of deactivated elements are excluded from the summations of model. An element's strain is also set to zero as soon as that element is killed. Similarly, when elements are 'born', they are not actually added to the model, but are simply reactivated. When an element is reactivated, its stiffness, mass, element loads, etc. return to their full original values.

2.1.3 Heat source model

For arc welding processes, the deposition of heat may be characterized as a distribution of heat flux on the weldment surface. Assuming that the heat from the welding arc is applied at any given instant of time as a normally distributed heat flux [**11**, **12**, **14**, **15**] then the rate of heat generation is given by

$$q_{sup}(r) = \frac{3Q}{\pi\bar{r}^2}\exp\left[-3\left(\frac{r}{\bar{r}}\right)^2\right] \qquad (5)$$

where $Q = \eta VI$, r is the distance from the centre of the heat source on the plate surface, and $\bar{r}$ is the characteristic radial dimensional distribution parameter that defines the region in which 95 per cent of the heat flux is deposited [**11**, **12**, **14**, **15**].

A heat source of suitable radius moving along the weld line at a particular speed can be used to model the welding process. The arc efficiency $(\eta = 0.90)$ [**11**, **13**] was taken to account for other losses. In SAW the arc is submerged with flux granules and the spread of the arc is difficult to observe. Hence, the arc radius of each job was selected on trial-and-error basis [**11**, **12**]. Various arc radii were tried to get an appropriate temperature distribution to match with the experiments. The arc radii used in the modelling for the SAW of double-sided fillets were 5.9 and 6.1 mm which were estimated by

considering the bead widths of the welds formed during experiments [11, 12].

2.2 Structural analysis

For evaluating the angular distortions, the heat transfer analysis was carried out first to find out nodal temperatures as a function of time. Then, in the second part of the analysis a thermomechanical non-linear elasto-plastic analysis was performed using the results obtained from the heat transfer analysis. The formulations for stress–strain evaluation used in the present study are

$$\boldsymbol{\sigma} = \mathbf{D}\boldsymbol{\varepsilon}^{e} \qquad (6)$$

where

$$\boldsymbol{\varepsilon}^{e} = \boldsymbol{\varepsilon} - \boldsymbol{\varepsilon}^{t} \qquad (7)$$

and

$$\boldsymbol{\varepsilon}^{t} = \Delta T \left[\alpha_x \ \alpha_y \ \alpha_z \ 0 \ 0 \ 0 \right]^{T} \qquad (8)$$

where $\Delta T = T_{n} - T_{\infty}$ and T_{n} is the instant temperature at the point of interest.

Considering the plastic strains, equation (7) can be written as

$$\boldsymbol{\varepsilon}^{e} = \boldsymbol{\varepsilon} - \boldsymbol{\varepsilon}^{t} - \boldsymbol{\varepsilon}^{p} \qquad (9)$$

The temperatures created by the welding of both sides of the fillet obtained from the thermal analysis were used as the thermal loadings in the structural analysis. The welding structural analysis involved large displacements (strain) and a rate-independent thermo–elasto–plastic material model with temperature-dependent material properties incorporated into the finite element modelling. Kinematic work hardening together with von Mises' yield criterion and associative flow rules [3, 5, 11] were assumed in the analysis. In the modelling eight-node brick elements were used for the thermal analysis and similar eight-node elements were used in the structural analysis. The eight-node brick elements were chosen to create the required compatibility level in the thermomechanical analysis. The solution was obtained using the ANSYS package [16].

3 MATERIAL PROPERTIES

The temperature-dependent material properties of the C-Mn steel used for the transient heat transfer and elasto-plastic analysis are given in Table 1 [3, 11, 12, 17]. The temperature-dependent enthalpy and yield stress values for steel are given in Tables 2 and 3 respectively [3, 11, 12, 17].

4 RESULTS AND DISCUSSIONS

4.1 Numerical thermal history of double-sided fillet during welding

3D finite element modelling for the welding of the double-sided fillet was performed for plates where

Table 1 Temperature-dependent material properties of C-Mn steel [3, 11, 12, 17]

Temperature (°C)	Thermal conductivity (W/mK)	Specific heat (J/kgK)	Thermal expansion coefficient (10^{-6}/°C)	Young's modulus (GPa)	Poisson ratio
0	51.9	450	10	200	0.2786
100	51.1	499.2	11	200	0.3095
300	46.1	565.5	12	200	0.331
450	41.05	630.5	13	150	0.338
550	37.5	705.5	14	110	0.3575
600	35.6	773.3	14	88	0.3738
720	30.64	1080.4	14	20	0.3738
800	26	931	14	20	0.4238
1450	29.45	437.93	15	2	0.4738
1510	29.7	400	15	0.2	0.499
1580	29.7	735.25	15	0.000 02	0.499
3500	42.1	400	15.5	0.000 02	0.499

Table 2 Temperature-dependent enthalpy for steel [11, 12]

	Temperature (°C)											
	0	100	200	300	400	500	600	700	800	900	1000	> 2500
Enthalpy (MJ/m^3)	0	360	720	1100	1500	1980	2500	3000	3700	4500	5000	9000

Table 3 Temperature-dependent yield stress for steel [3, 11, 12, 17]

	Temperature (K)							
	293	373	573	773	973	1073	1273	1473	1673
Yield stress (σ_y) (MPa)	398	379	305	192	41	36	28	20	12

melting temperature is 1495°C [12, 17] and A_1 transformation temperature is 723°C [12, 17]. For the finite element modelling brick elements were taken with fine meshing in the weld zone. In the present analysis, after completion of the welding of one side the second side was welded. For this reason the transient thermal histories i.e. temperature distribution with time are different for the two sides of the plate. The results of the transient thermal analysis are shown in Figs 2 and 3 respectively. Figure 2 shows the temperature distribution of the first side of the fillet during welding (i.e. the area bounded by weld lines 1-2-4-3-1 in Fig. 1) and Fig. 3 shows the temperature distribution of the second side of the fillet during welding (i.e. the area bounded by weld lines 5-6-8-7-5 in Fig. 1) respectively, as a function of distance from the line 2–4. Figure 2 shows that the temperature profile for the moving heat source shoots up to nearly 1800°C at the middle of the first fillet weld area (i.e. area bounded by weld lines 1-2-4-3-1 in Fig. 1) and that cooling occurs up to 185 s. The second welding operation (i.e. area bounded by weld lines 5-6-8-7-5 in Fig. 1) begins after the cooling of the first weld but it results in the temperature profiles for the first fillet increasing again in this case up to nearly 630°C as shown in Fig. 2. This indicates post-welding heating of the first fillet weld caused by the second welding operation. Figure 3 shows the temperature distributions for the second welding operation which are affected by the first welding operation to the extent that the second side of the fillet is preheated up to a temperature of nearly 420°C. The timescale for Fig. 3 also includes the timescale for heating and cooling of the first fillet weld. The parameters used for double-sided fillet welding are given in Table 4. Even though the same welding parameters are used for the welding of both sides of the fillet the peak welding temperature is nearly 2100°C for the second side of the fillet because the joint is already preheated by the welding of the first side of the fillet (Fig. 3).

4.2 Distortion during the double-sided fillet welding

Figures 4 and 5 show the distortion patterns for 10 mm thick plates obtained after welding using the parameters listed in Table 5. In the finite element modelling the angular distortions were plotted based on the nodal deflections from the non-linear
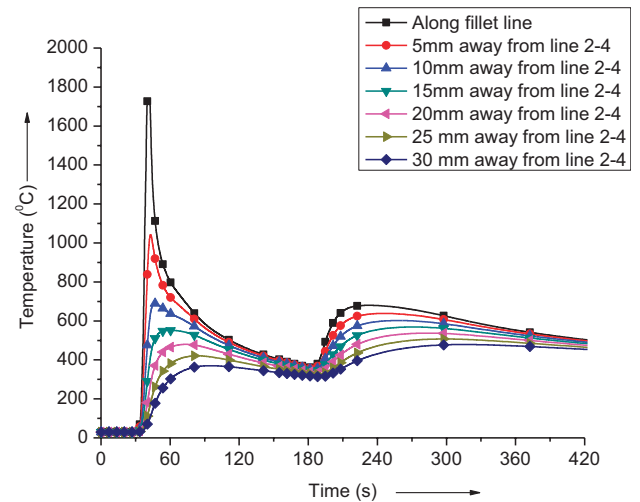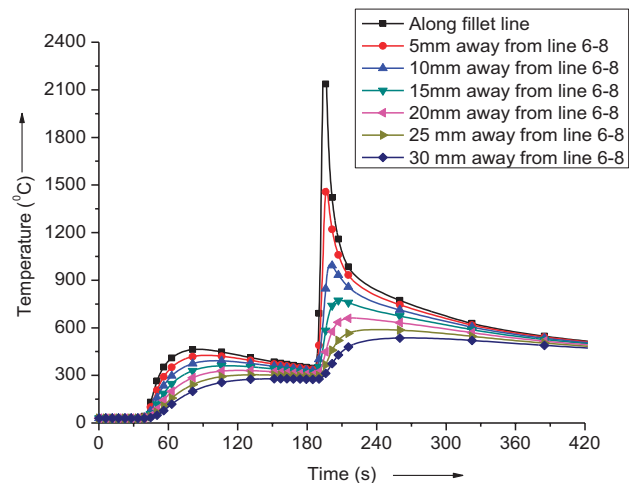

Fig. 2 Temperature distribution at various points on the top surface of the plate for the welding of the first side of the fillet

Fig. 3 Temperature distribution at various points on the top surface of the plate for the welding of the second side of the fillet

Table 4 The experimental conditions used for the welding of both sides of the fillet

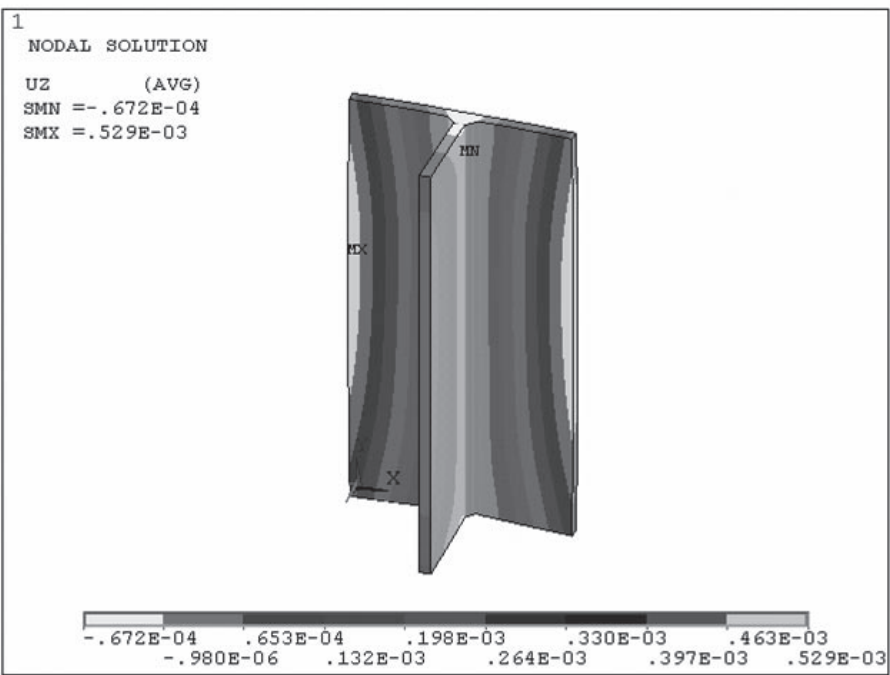|	Welding parameters		
Plate thickness (mm)	Current (A)	Voltage (V)	Speed (mm/s)
10	420	25	5.0

Fig. 4   Distortion pattern for a 10 mm thick plate under the welding parameters listed in Table 5 for Job.1
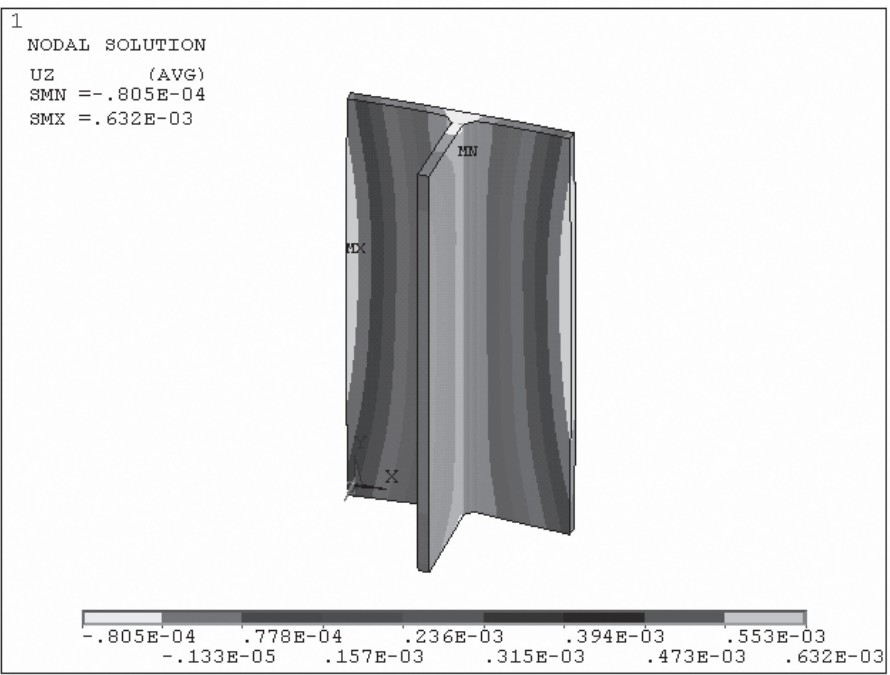

Fig. 5   Distortion pattern for a 10 mm thick plate using the welding parameters listed in Table 5 for Job.2

elasto–plastic analysis at the edges (13-14-20-19 and 11-12-18-17 in Fig. 1) of the fillet joint models. Figure 6 shows a comparison of the finite element angular distortions (nodal deflections) at the edges (i.e. 13-14-20-19 and 11-12-18-17 in Fig. 1) of the joint models for the welding parameters given in Table 5.

Table 5   Welding parameters for the double-sided fillet welding

Job	Thickness (mm)	Current (A)	Voltage (V)	Welding speed (mm/s)
1	10	425	25	5.0
2	10	460	27	5.0

4.3 Experimental details of SAW double-sided fillet welding

In order to measure the temperature distribution thermocouples were placed 15 mm away from the weld line on the upper surfaces of the plates during the welding operations. The data from the thermocouples were acquired using an Agilent data logger. The chemical composition of the steel is given in Table 6.

Single-run SAW was carried out using a 1200 A constant voltage DC power source with a 4 mm diameter electrode and positive polarity. The contact tube to the workpiece distance was kept at 30 mm for all samples.

After welding, each sample was cross-sectioned, polished to a 1 μm finish using silicon carbide paper, and etched in a 2 per cent Nital solution [11, 12, 17]. Two etched sections are shown in Figs 7 and 8 respectively.

Before welding the fillet was tack welded to the base plate as per the scheme of tack welding positioning given in Mahapatra *et al.* [11]. Then, initial measurements of the plate top surface at the predefined locations were taken with respect to a fixed datum using a linear variable differential transformer (LVDT) [11]. The LVDT was mounted on a suitable carriage with three degrees of motion. Subsequently, welding was carried out using SAW. After the plate cooled down to ambient temperature, plate surface measurements were taken at the previously defined locations using the LVDT. The difference between the measurements taken before and after the welding operations indicated the actual distortion of the welded plate.
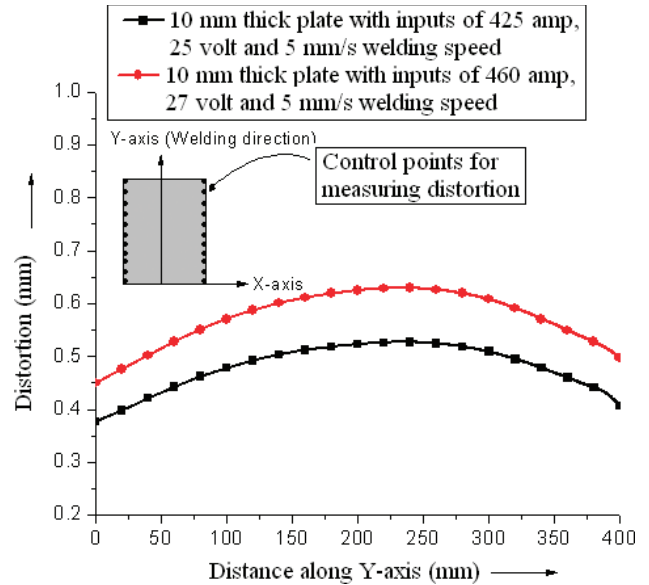

Fig. 6 Comparison of the angular distortions near the end of the welded plate and parallel to the weld line using the conditions listed in Table 5

Table 6 Chemical composition of the C-Mn steel (percentage)

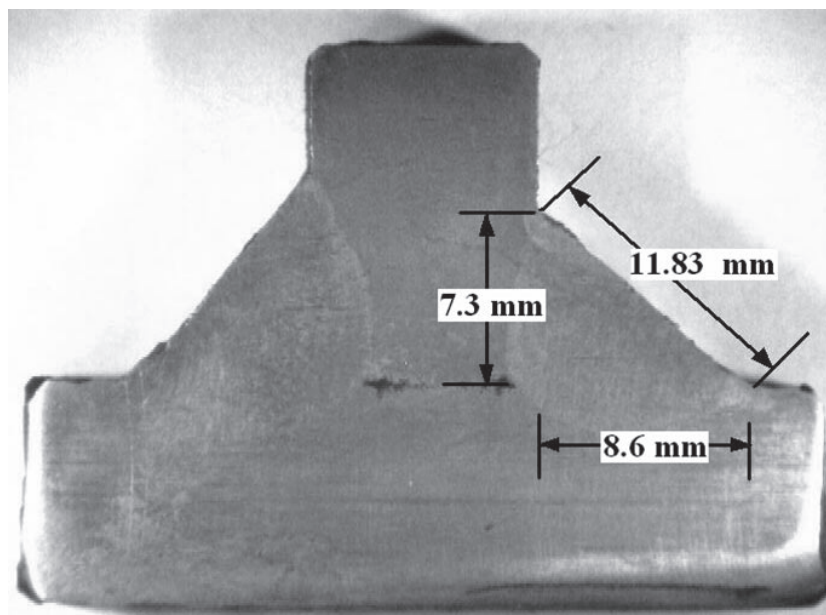| C	Si	Mn	P	S	Cr	Ni	Mo	Cu	Al
0.19	0.37	1.57	0.023	0.027	0.06	0.03	0.01	0.04	0.046

Fig. 7 Etched section of the double-sided fillet after welding performed at 425 A, 25 V, and a 5.64 mm/s welding speed
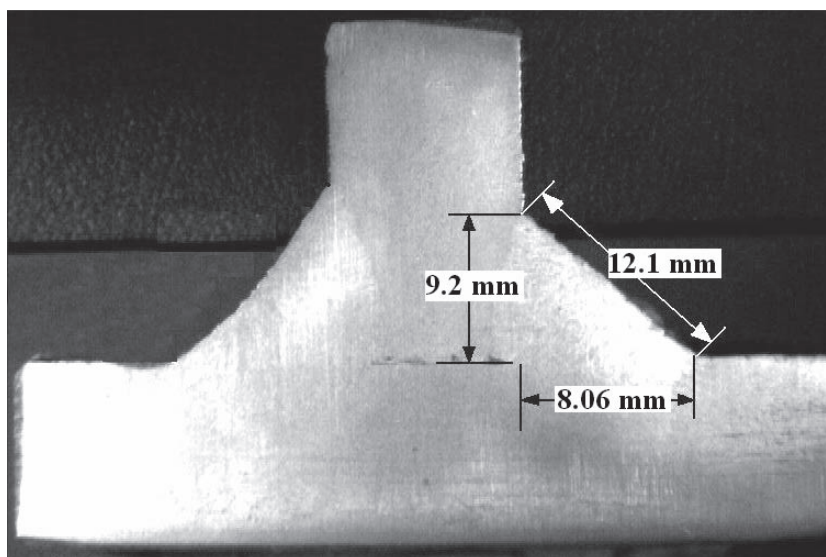
Fig. 8 Etched section of the double-sided fillet after welding performed at 470 A, 27 V, and a 5 mm/s welding speed

4.4 Verification of experimental and calculated thermal profiles

Figure 9 shows the experimental and calculated thermal profiles. The experimental points (thermocouple position) for the thermal history were located 15 mm away from the (for the first side fillet weld) weld line 2-4 (Fig. 1) on the top surface of the horizontal plate at a distance of 200 mm from the edge 9-10-11-12-13-14 (Fig. 1). The input welding parameters of this thermal profile (Fig. 9) are given in Table 7. A comparison of the experimental and calculated thermal profiles for the input welding parameters given in Table 7 is shown in Fig. 9. It can be observed from Fig. 9 that there is a close agreement between the experimental and calculated thermal profiles.
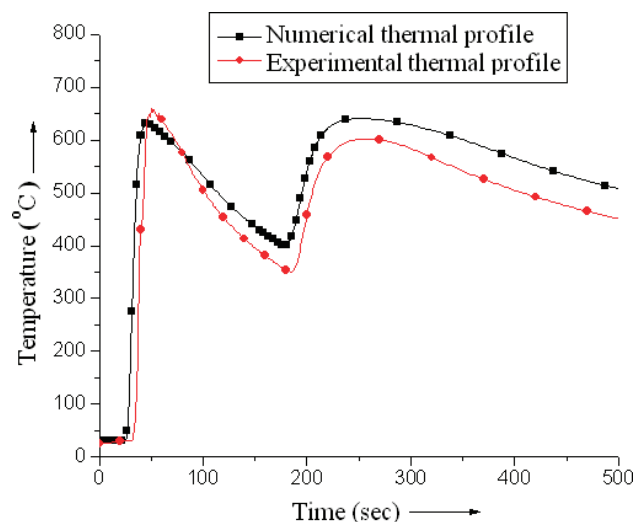
4.5 Verification of experimental and numerical distortion

The used experimental parameters for the SAW process are given in Table 8. Figure 10 shows the control points of the double-sided fillet welding for distortion measurements. Figure 11 shows the experimental and calculated welding distortion patterns for the 10 mm thick plate using the conditions for job 1 listed in Table 8. Figure 12 shows the experimental and calculated distortion patterns for the 10 mm thick plate using the conditions for job 2 listed in Table 8. From Figs 11 and 12 it can be observed that there is close agreement between the experimental and calculated distortions.

The methodology developed in the present investigation can be considered adequate for predicting the temperature distributions and resulting angular distortions. In SAW the arc is covered by the flux

Fig. 9 A comparison of the experimental and calculated thermal profiles

Table 7 Experimental welding parameters used in the double-sided fillet welding

Thickness (mm)	Length of stick out (mm)	Current (A)	Voltage (V)	Welding speed (mm/s)
10	30	470	27	5.0

Table 8 Experimental welding parameters used in the double-sided fillet welding

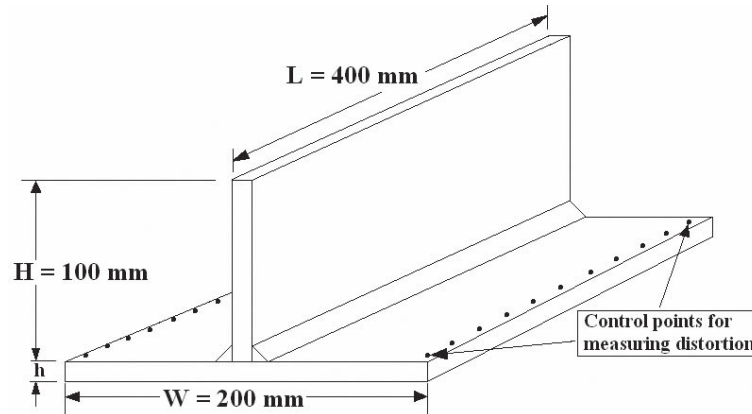| Job	Thickness (mm)	Length of stick out (mm)	Current (A)	Voltage (V)	Welding speed (mm/s)
1	10	30	425	25	5.64
2	10	32	470	27	5.0

Fig. 10 Plate dimensions and control points for the distortion measurements (*W* is the width of the plate along the *X*-axis, *L* is the total length along the *Y*-axis, and *h* is the thickness of the plate)
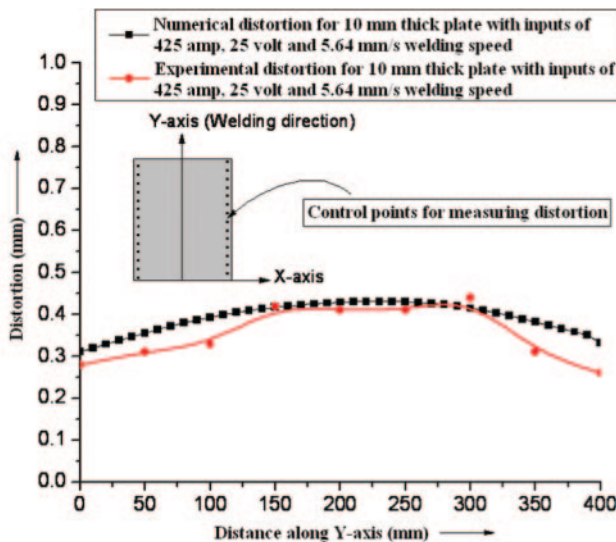

Fig. 11 Comparison of the experimental and calculated angular distortions for the welding parameters for job 1 listed in Table 8
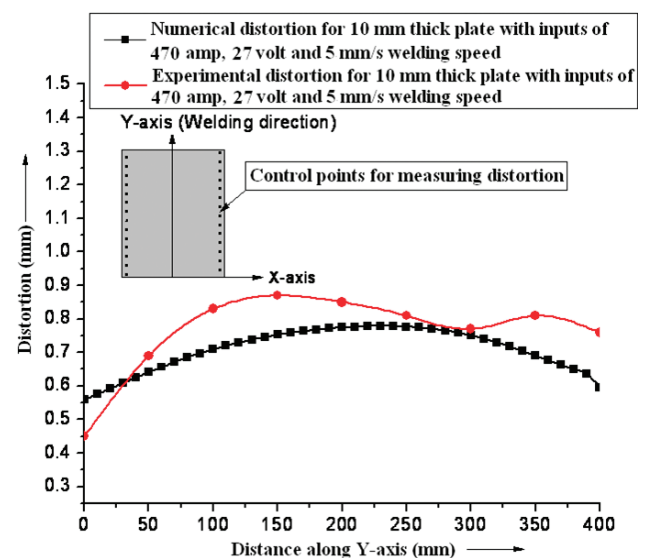

Fig. 12 Comparison of the experimental and calculated angular distortions using the welding parameters for job 2 listed in Table 8

granules so that the nature of the arc spread is difficult to observe. The methodology developed in the present investigations is based on a moving SAW heat flux and is able to predict the temperature distributions and angular distortions.

5 CONCLUSIONS

The following conclusions can be drawn from the present investigations.

1. A 3D finite element model for the double-sided fillet SAW process was developed and successfully compared with the experimental results.
2. The temperature distributions obtained through analysis and those obtained from experimental measurements compared fairly well with a variation of only 8 per cent for the peak temperatures.

3. The angular distortions obtained through the finite element analyses and those obtained from experimental measurements compared fairly well with a variation of 5–10 per cent only, for the maximum distortions.

© Authors 2010

REFERENCES

1 **Rosenthal, D.** Mathematical theory of heat distribution during welding and cutting. *Weld. J.*, 1941, **21**(5), 220s–234s.
2 **Rosenthal, D.** The theory of moving sources of heat and its application to metal treatments. *Trans. AIME*, 1946, **43**(11), 849–866.

3 **Brown, S.** and **Song, H.** Implication of three-dimensional numerical simulation of welding of large structures. *Weld. J.*, 1992, 55s–62s.

4 **Kamala, V.** and **Goldak, J. A.** Error due to two dimensional approximation in heat transfer analysis of welds. *Weld. J.*, 1993, **72**(9), 440s–446s.

5 **Michaleris, P.** and **DeBiccari, A.** Prediction of welding distortion. *Weld. J.*, 1997, **76**(4), 172s–180s.

6 **Tsai, C. L.** and **Cheng, W. T.** Welding distortion of thin-plate panel structures. *Weld. J.*, 1999, **78**(5), 156s–165s.

7 **Teng, T.-L., Fung, C.-P., Chang, P.-H.,** and **Yang, W.-C.** Analysis of residual stresses and distortions in T-joint fillet welds. *Int. J. Press. Vessels Pip.*, 2001, **78**, 523–538.

8 **Tsai, C. L.** and **Jung, G. H.** Plasticity-based distortion analysis for fillet welded thin-plate T-joints. *Weld. J.*, 2004, **83**(6), 177s–187s.

9 **McDill, J. M. J., Oddy, A. S.,** and **Goldak, J. A.** Comparing 2-D plane strain and 3-D analyses of residual stresses in welds. In Proceedings of the third International Conference on *Trends in welding research*, 1993, pp. 105–108 (ASM International, Materials Park, OH).

10 **Murakawa, H., Serizawa, H.,** and **Shibahara, M.** Prediction of welding hot cracking using temperature dependent interface element – modelling of interfaces. *Math. Model. Weld Phen.*, 2005, **7**, 539–554.

11 **Mahapatra, M. M., Datta, G. L., Pradhan, B.,** and **Mandal, N. R.** Modelling the effects of constraints and single axis welding process parameters on angular distortions in one-sided fillet welds. *Proc. IMechE, Part B: J. Engineering Manufacture*, 2007, **221**(B3), 397–407. DOI: 10.1243/09544054JEM617.

12 **Pathak, A. K.** and **Datta, G. L.** Three-dimensional finite element analysis to predict the different zones of microstructures in submerged arc welding. *Proc. IMechE, Part B: J. Engineering Manufacture*, 2004, **218**(B3), 269–280. DOI:10.1243/095440504322984821.

13 **Okada, A.** Application of melting efficiency and its problems. *J. Jpn Weld. Soc.*, 1977, **46**, 53–61.

14 **Fanous, F. Z. I., Younan, M. Y. A.,** and **Wifi, S. A.** 3-D finite element modelling of the welding process using element birth and element movement techniques. *Trans. ASME, J. Press. Vessel Technol.*, 2003, **125**, 144–150.

15 **Friedman, E.** Thermo mechanical analysis of the welding process using the finite element method. *Trans. ASME*, 1975, 206–213.

16 Ansys, Inc. Theory reference, Ansys Inc., 2002.

17 **Mandal, N. R.** and **Adak, M.** Fusion zone and HAZ prediction through 3-D simulation of welding thermal cycle. *J. Mech. Behav. Mater.*, 2001, **12**(6), 401–414.

APPENDIX

Notation

c	specific heat (J/kg K)
$\boldsymbol{D}$	stress strain matrix
h_f	convective heat transfer coefficient (W/m^2 K)
k	thermal conductivity (W/m K)
q_n	component of conduction heat flux normal to the work surface (W/m^2)
q_{sup}	supplied heat flux from the welding arc (W/m^2)
q_{conv}	heat loss from the work surfaces by convection (W/m^2)
Q	arc power (W)
r	radial distance in the welding arc (mm)
S_1 and S_2	surfaces
t	time (s)
T	temperature (°C)
T_∞	temperature of the surroundings (°C)
x, y, z	coordinates
$\alpha_x, \alpha_y, \alpha_z$	thermal expansion coefficients in x, y, and z coordinates
$\boldsymbol{\varepsilon}$	total strain vector
$\boldsymbol{\varepsilon}^e$	elastic strain vector
$\boldsymbol{\varepsilon}^p$	plastic strain vector
$\boldsymbol{\varepsilon}^t$	thermal strain vector
η	arc energy transfer efficiency
ρ	density of the base metal (kg/m^3)
$\boldsymbol{\sigma}$	stress vector